Strong-magnetic-field behavior of small-particle superconducting composites

D. J. Resnick* and J. C. Garland
Department of Physics, Ohio State University, Columbus, Ohio 43210

F. P. Esposito and R. S. Newrock
Department of Physics, University of Cincinnati, Cincinnati, Ohio 45221
(Received 9 September 1983)

The influence of isolated superconducting inclusions on the magnetoresistance of a normal-metal host is calculated using a phenomenological current-distortion model. We find a linear enhancement of the magnetoresistance that can be identified with large distortions of the current flow in the normal-metal region immediately surrounding each inclusion. Our calculations are compared with existing experimental results.

I. INTRODUCTION

Composite superconductors, consisting of random arrays of superconducting particles embedded in insulating or normal metal hosts, exhibit a variety of interesting properties when the volume fraction of superconductor is below the percolation threshold. Most recent work on these materials has been performed in zero magnetic field and has centered on the effects of Josephson coupling between isolated superconducting grains. For example, studies of NbN (Ref. 1), HgXe (Ref. 2), and PbZn (Ref. 3) composites have revealed a rich variety of dimension-dependent transport effects.

In recent papers Resnick, Garland, and Newrock[4] (RGN) showed that random superconducting-normal metal (S/N) composites also exhibit interesting transport behavior in strong magnetic fields. Their principal result is that the presence of superconducting NbTi grains in a normal In host increases the magnetoresistance—and consequently the joule dissipation—of the material. Unlike zero-field transport effects, this high-field behavior is inherently classical in nature; the Josephson effect and proximity coupling effects are suppressed completely in strong magnetic fields. Stroud[5] has recently proposed that the high-field resistivity could be explained by a generalized effective medium theory which takes into consideration the symmetry and field dependence of the conductivity tensor of the normal-metal constituent. His calculations show that the resistivity increases as a linear function of the superconducting volume fraction, consistent with the measurements of RGN.

The purpose of this paper is to develop this result, namely, that the resistivity is a linear function of the superconducting volume fraction, by demonstrating that the resistivity enhancement may be identified with the distortion of the current density in the normal-metal medium. A surprising result of our study is that the volume within which this current distortion occurs is much larger than the volume of the inclusion which induced the distortion. This finding is to be contrasted with the zero-field situation, where current distortion effects are localized to the immediate volume surrounding the inclusion.

II. PHENOMENOLOGICAL MODEL FOR S/N COMPOSITES

Our model of a S/N composite is a collection of widely spaced superconducting spheres embedded in a free-electron normal metal host. The radii of the spheres are assumed to be much larger than the electron mean free path l, the cyclotron radius R_c, and the superconducting coherence length ξ. The first two of these inequalities permit us to treat current flow in the normal metal as a hydrodynamic process in which the current at each point is specified uniquely by the conductivity and the local electric field. While this assumption makes it possible to account for sharp field gradients without invoking the mathematical complexities of nonlocal transport theory, it also restricts the applicability of our results to bulk (three-dimensional) superconducting particles in which fluctuation effects are unimportant.

Finally, we assume that the superconducting particles are in the extreme type-II limit. In this limit, magnetic flux readily penetrates the spheres, allowing us to treat them as classical objects having perfect conductivity. A result of this assumption is that our model cannot generate correct current profiles in the interior of the superconducting spheres. This is an unimportant liability since there is no dissipation within the spheres. The current profiles in the normal metal are not affected by this assumption.

It is reasonable to ask whether our model will yield an accurate explanation of the experimental results of RGN. The model cannot produce the correct current distribution patterns at low fields, characterized by $\omega_c\tau \ll 1$, where ω_c is the cyclotron frequency and τ is the electron mean scattering time in the normal metal. In this low-field regime the conductivity of a "real" normal metal departs significantly from the simple free-electron conductivity we have assumed. In practice, the magnetic field corresponding to $\omega_c\tau \ll 1$, is also likely to be below H_{c1} of the superconducting inclusions. Below H_{c1}, the diamagnetic screening currents on the surfaces of the inclusions severely disturb the homogeneous magnetic field distribution as-

sumed in our calculations. Finally, our model is applicable only to the very dilute limit, where the superconducting volume fraction $f \ll 1$. In concentrated superconducting-normal composites the distortion of the current flow is much more complicated than our model predicts because of interactions between the current streamlines around closely spaced inclusions. As will be shown below, the boundary between the dilute limit, where our model is accurate, and the nondilute limit, where it is not, scales with the magnetic field. At sufficiently strong magnetic fields, therefore, any real sample will eventually move into the nondilute regime.

The calculations are done in the following manner. We consider a single, isolated superconducting sphere located at the origin. The applied magnetic field is parallel to the $\hat{z}$ axis and the injected current is parallel to either the $\hat{x}$ axis (transverse case) or $\hat{z}$ axis (longitudinal case). We obtain the lines of electric current near the inclusion by solving Laplace's equation for the electrostatic potential, $\Phi(r)$, using the constitutive equation

$$J^i=\sigma^{ij}E_j \ , \tag{1}$$

where σ^{ij} are components of $\sigma(h)$, the field-dependent conductivity tensor of the normal metal, given by

$$\sigma(h)=\sigma_0\begin{bmatrix} \gamma & h\gamma & 0 \\ -h\gamma & \gamma & 0 \\ 0 & 0 & 1 \end{bmatrix} . \tag{2}$$

In the above equation, $h=\omega_c\tau$ and $\gamma=(1+h^2)^{-1}$. In a strong magnetic field $h \gg 1$, $\gamma=1/h^2$ and σ_{xx} and σ_{yy} are much smaller than σ_{zz}. The conductivity tensor thus becomes extremely anisotropic at high fields; this anisotropy is responsible for the unusual features of this problem. Because of the low transverse conductivity, there is a marked tendency for a current streamline in the $\hat{x}$ direction, if perturbed by an inclusion, to travel a considerable distance along the higher conductivity $\hat{z}$ direction.

The boundary value equation can be obtained from

$$-\nabla_i J^i=\nabla_i\sigma^{ij}\nabla_j\Phi=0 \ .$$

Because the procedure used to solve this equation is relatively well known,[6,7] we give here only a brief summary. We first apply a scale transformation to the z coordinate, $z'=z/(1+h)^{1/2}$, which reduces the above differential equation to Laplace's equation. In the scaled coordinate system all characteristic dimensions of the problem parallel to the applied magnetic field are compressed by a factor approximately equal to $1/h$, transforming the spherical inclusion into an oblate spheroid. We then obtain the solution to Laplace's equation in oblate spheroidal coordinates and transform the results back to rectangular coordinates to obtain the potential, electric field, and current distribution.

There are two boundary conditions: at the normal-metal–superconductor interface (i.e., the surface of the superconducting inclusion) the electric potential is zero, while far from the inclusion the electric potential, or alternately, the current density, is uniform. Although these boundary conditions uniquely determine the current and electric field patterns outside the inclusion, they do not specify the solution inside. For example, the solutions do not distinguish between perfectly conducting inclusions and superconducting inclusions. In the former case the current density is uniform, while in the latter current flows within a penetration depth of the surface. We note also that because the angles between vectors are not preserved during the scale transformation, the treatment of the boundary conditions is fairly complicated. Interested readers can refer to Refs. 6 and 7 for additional details.[8]

III. RESULTS OF THE CALCULATIONS

For the transverse magnetoresistance ($J=J_{0x}$ for $r \gg R$), the electric potential we obtain is

$$\Phi_T=\frac{\alpha J_0}{\sigma_0}\sin\theta(\cos\phi+h\sin\phi) \times\left[\frac{\cosh\eta_0}{Q_1^1(i\sinh\eta_0)}-\cosh\eta\right] . \tag{3}$$

For the longitudinal case ($J=J_{0z}$ for $r \gg R$), we obtain

$$\Phi_L=\frac{\alpha J_0}{\gamma^{1/2}\sigma_0}\left[\frac{\sinh\eta_0}{Q_1(i\sinh\eta_0)}Q_1(i\sinh\eta)-\sinh\eta\right] . \tag{4}$$

In each of the above equations η,θ,ϕ are oblate spheroidal coordinates, defined from the scaled coordinate system $r'=(x',y',z')$ by

$$\begin{aligned} x'&=\alpha\cosh\eta\sin\theta\cos\phi \ , \\ y'&=\alpha\cosh\eta\sin\theta\sin\phi \ , \\ z'&=\alpha\sinh\eta\cos\theta \ . \end{aligned} \tag{5}$$

In Eqs. (3)–(5), $Q_1(z)$ is the associated Legendre polynomial of the second kind, $\alpha=Rh\gamma^{1/2}$, $\sinh\eta=1/h$, $Q_1^1(z)=(z^2-1)(d/dz)Q_1(z)$, and $z=i\sinh\eta$. The expressions for the currents may be obtained from the potentials and are summarized in the Appendix.

Computer-generated "maps" of the current lines and the local joule dissipation for the longitudinal and transverse magnetoresistance are shown in Figs. 1–5. The computer algorithm first calculates the magnitude and the direction of the current density at a point far from the inclusion in a region where the current density is uniform. It then calculates the magnitude and direction at a second point a small step from the first along the direction of the current. This process is repeated until the entire current line is mapped out. The procedure is then iterated as often as necessary to map out all the current lines. The size of the steps is kept sufficiently small so that the cumulative error is negligible.

Figures 1 and 2 show the computer-generated trajectories in the transverse case ($\vec{J}\perp\vec{H}$) for several lines and sheets of electric current. Figure 1(a) shows representative current trajectories projected onto the $\hat{x}$-$\hat{z}$ plane ("side view"), and Fig. 1(b) shows the same trajectories projected onto the $\hat{x}$-$\hat{y}$ plane ("top view"). In both cases $h=100$. Figure 2 is an isometric projection of several sheets of current for $h=10$. There are a number of interesting features in these figures. First, the current tends to avoid

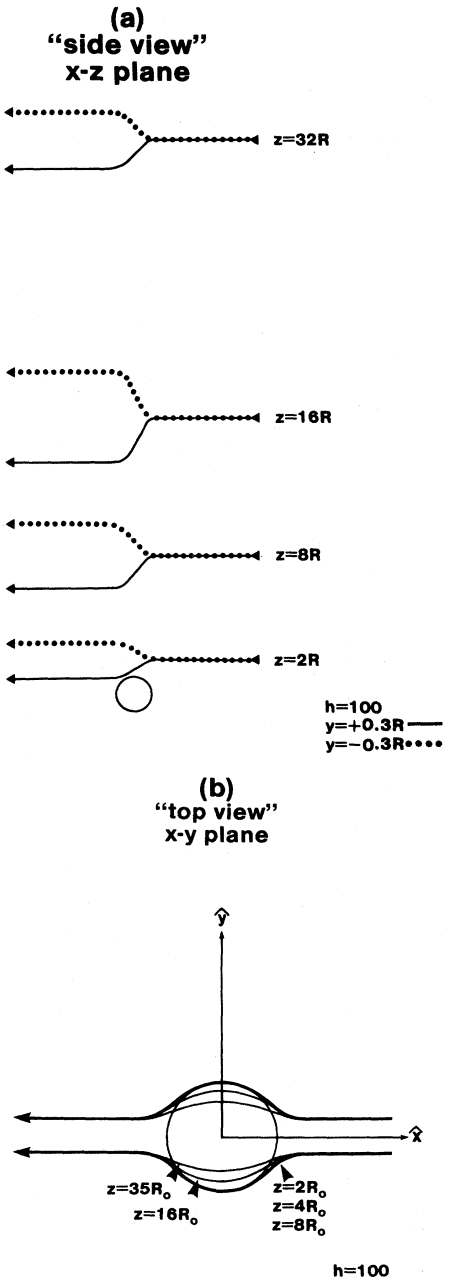

FIG. 1. Computer-generated trajectories for ($\vec{J} \perp \vec{H}$) for lines of electric current at various distances above superconducting inclusion. (a) "side view": trajectories projected onto the $\hat{x}$-$\hat{z}$ plane; (b) "top view": trajectories projected onto the $\hat{x}$-$\hat{y}$ plane. In both cases the reduced field $h = 100$.

the "shadow" region in the normal metal above and below the sphere (see the inset in Fig. 2). Second, in strong fields, significant current distortion extends a distance on the order of hR on either side of the inclusion, along the direction of the field. By contrast, in zero field the region of current distortion is only about $2R$. Third, there is a significant assymmetry to the current flow. In the upper half-plane, the current sheet divides into two parts. Over one hemisphere of the inclusion it veers upward away from the inclusion, whereas over the other it veers downward toward it (Fig. 2). This division is reversed in the lower half-plane.

Additionally, those current lines which pass very close to the sphere are pulled toward it and enter the region near the equator. (In the limit of an infinitely strong magnetic field, the current lines are able to enter the sphere only at its equator.) Finally, the current which is excluded from the shadow region is compressed into a thin cylindrical shell which defines the shadow perimeter (Fig. 2, inset). It is this region of high current density which is responsible for most of the magnetoresistance observed by RGN.

The effects of this high-density region on the magnetoresistance are illustrated in Fig. 3, which shows several isometric projections of the dissipation, $\vec{J} \cdot \vec{E}$. In the figure, the dissipation is shown on the vertical axis while the $\hat{x}$-$\hat{y}$ axes specify a particular plane at fixed z above the inclusion. Figure 3(a) shows $\vec{J} \cdot \vec{E}$ for $h = 10$, 50, and 100 in the plane $z = 2$, while Fig. 3(b) shows $\vec{J} \cdot \vec{E}$ for $h = 100$ at various distances, $z/R = 2$, 4, 8, and 16, above the sphere. Although the dissipation is most pronounced in strong fields, it is clear that even in moderate fields the excess joule heating is significant. We notice that the largest field shown, $h = 100$, is readily attainable in a pure metal at low temperatures.

To obtain the total dissipation in the specimen, we integrate $\vec{J} \cdot \vec{E}$ over the volume of the specimen. For low volume fraction of superconductor we find that $\rho = (1.3)h$, in agreement with direct calculations from effective medium theory. The transverse magnetoresistivity is thus seen to be linear in the applied magnetic field, with no saturation as long as the composite stays in the dilute limit. This result may be compared to the similar geometry for a void where a linear magnetoresistivity is also seen[6,7] with a slope of the same order of magnitude.

Figures 4 and 5 show examples of the current trajectories and local dissipation for the longitudinal case (i.e., for the current parallel to the applied magnetic field). Figure 4 displays several representative trajectories for current injected in the $\hat{x}$-$\hat{z}$ plane. For this case, the distortion in the trajectories is largest when the reduced field is zero. The distortion begins to decrease as the reduced field approaches one, and continues to decrease, until, for large h, almost no distortion is discernable.

The distortions of the current patterns are mirrored in the local joule dissipation. In Fig. 5 we have plotted $\vec{J} \cdot \vec{E}$ in the plane $z = 2$. For zero and low fields, the distortion produces a large dissipation peak centered over the sphere. As the applied field increases, this dissipation peak becomes progressively smaller, until, at very high fields, it is barely discernable. Surprisingly, however, the decrease in the local dissipation does not lead to a decrease in the total resistance of the specimen. This apparent inconsistency is resolved by comparing the results for the resistance in the two extremes of applied field. It is a well-known result of effective medium theory[9] that in zero field, $\rho(h=0) = \rho_0(1 - 3f)$. This equation expresses the idea that the extra dissipation induced by current bending in

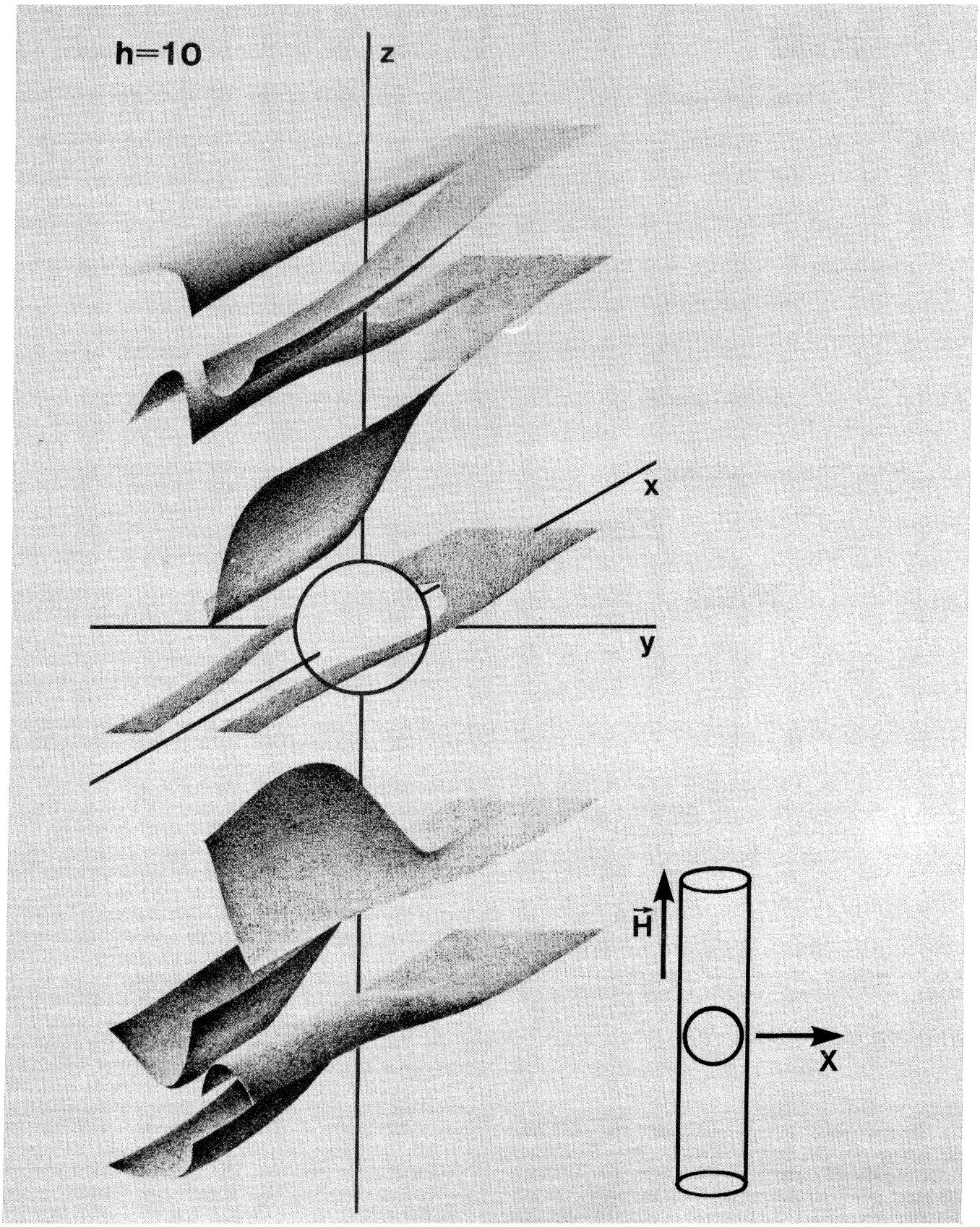

FIG. 2. Computer-generated isometric projection of several sheets of current for reduced field $h = 10$.

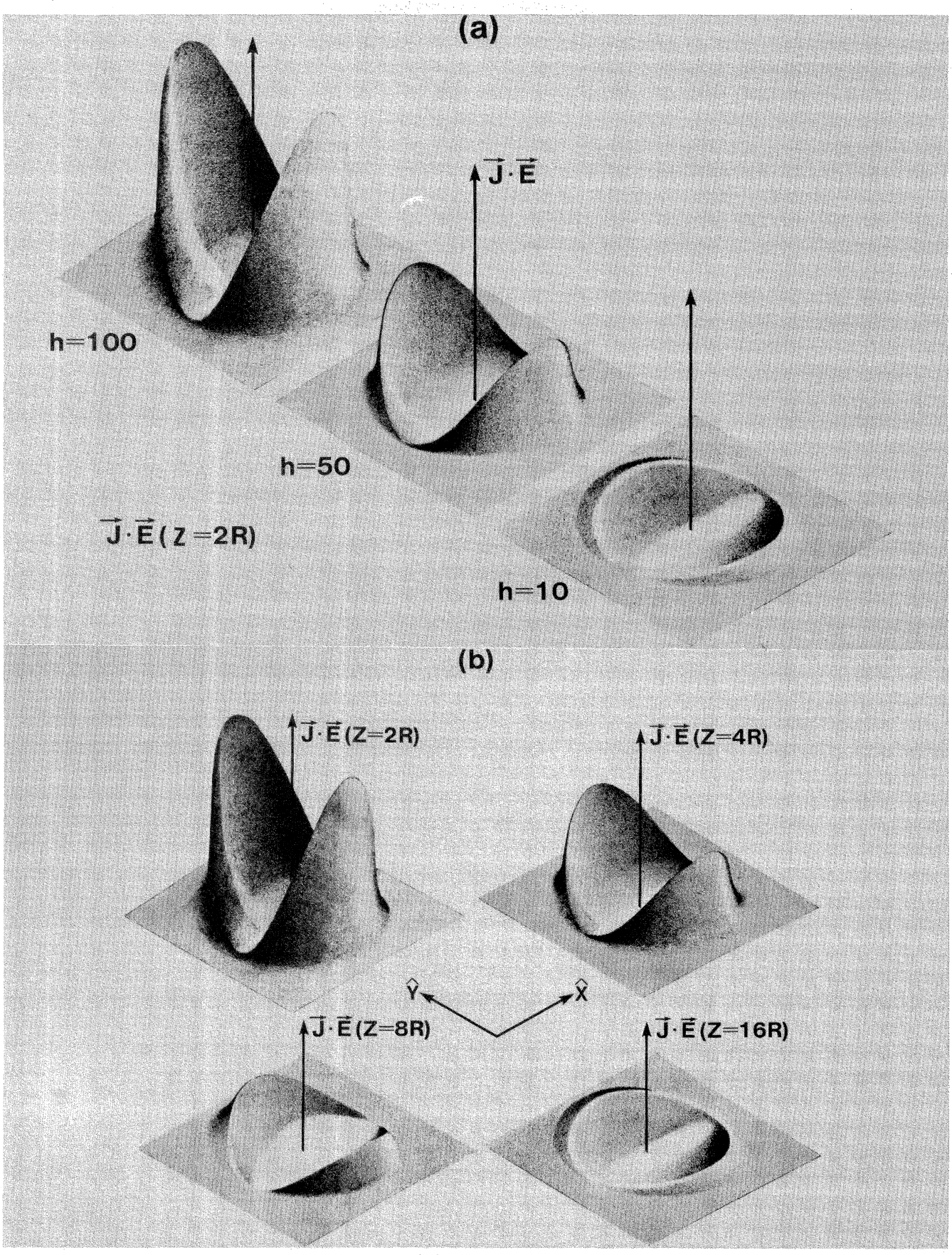

FIG. 3. Isometric projection of the power dissipated ($\vec{J}\cdot\vec{E}$) in the neighborhood of the inclusion for the transverse case. (a) $\vec{J}\cdot\vec{E}$ for various h in the plane $z=2$; (b) $\vec{J}\cdot\vec{E}$ for various z at $h=100$.

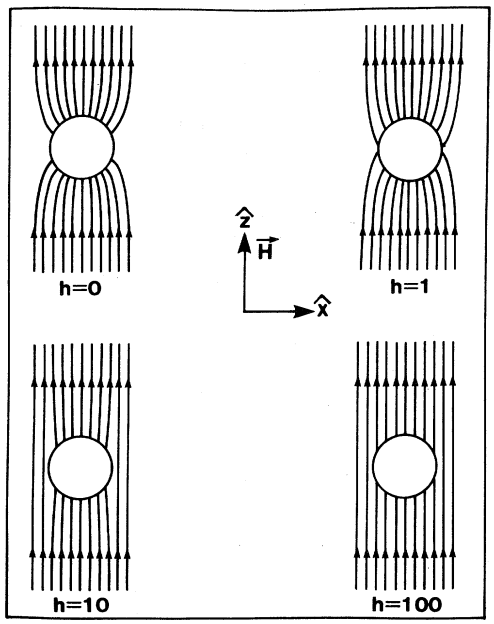

FIG. 4. Current trajectories for the longitudinal case ($\vec{J}||\vec{H}$) for several values of the reduced field.

toward each inclusion is more than compensated by the resistanceless flow of current in the interior of the inclusion. In the very-high-field limit, however, the analogous expression[5,7] is $\rho(h=\infty,f)=\rho_0(1-f)$, a result that might be anticipated from the absence of high-field distortion in Fig. 4. In this limit, the total resistance is simply that of a metal with uniform current density and a volume fraction f of zero resistance inclusions. Although the net effect of the field is to reduce the current distortion created by the inclusions, this reduction increases the resistance because it results in less total current flow inside the resistanceless regions. This result may be contrasted with the results for a spherical void, where the current spirals around the ouside of the void, resulting in the formation of a high-density current sheet with large dissipation.[6]

IV. DISCUSSION AND SUMMARY

The free-electron conductivity tensor [Eq. (1)] accurately reflects the high-field magnetoresistance of simple metals (metals which are uncompensated with closed Fermi surfaces). In the high-field limit ($h=\omega_c\tau\gg1$), the conductivity parallel to the field is unchanged but the conductivity perpendicular to the field is reduced by a factor of $1/h^2$. It is well known that in a homogeneous pure metal

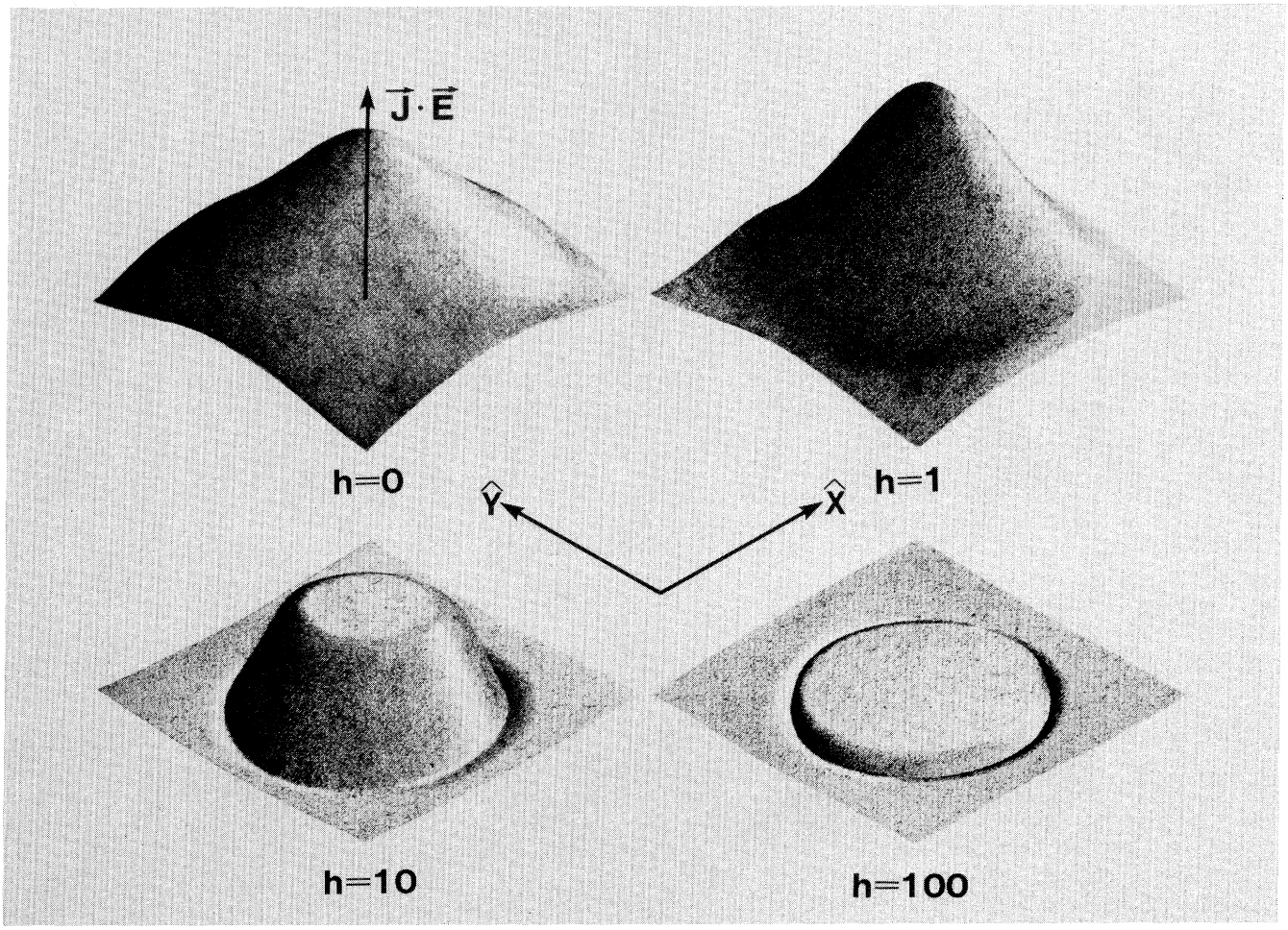

FIG. 5. Isometric projection of the dissipation $\vec{J}\cdot\vec{E}$ in the neighborhood of the inclusion for the longitudinal case.

this large anisotropy does not produce any additional dissipation. Therefore, if a superconducting inclusion is present, the large linear increase in the resistance with field (for $\vec{J}\perp\vec{H}$) is solely a result of the current distortion. In S/N composites, this increase in the resistance more than compensates for the lowering of the bulk resistivity caused by the addition of superconductor, and we have the interesting result that the addition of superconducting material to a normal metal increases the resistance.

These results apply only to S/N composites whose concentration of inclusions is sufficiently dilute that the current distortion regions around each inclusion remain isolated from one another. Because the region of current distortion increases with increasing magnetic field, however, the dilute regime is determined both by the volume fraction of inclusions and by the magnetic field strength. At sufficiently strong fields, our model fails because the current distortion regions from adjacent inclusions begin to overlap. We may estimate this maximum field by noting that current distortions are essentially confined to the cylindrical shadow of the inclusion (inset, Fig. 2), which has a volume

$$V_s=\frac{\pi D^3(1+h^2)^{1/2}}{2}\cong\frac{\pi}{2}D^3h \ ,$$

where D is the diameter of the inclusion and $2D(1+h^2)^{1/2}$ is the length of the shadow. In the dilute limit, the increase of the apparent resistivity with field is proportional to the fraction of the specimen volume over which the shadow extends. Thus we can set

$$\rho(f,h)\propto\frac{NV_s}{V}\propto\frac{ND^3}{V}(1+h^2)^{1/2}\cong fh \ ,$$

where N is the number of inclusions in a specimen of volume V. The resistance is linear in f and h as long as $(NV_s/V)\ll 1$. As f or h is increased, so that $(NV_s/V)\approx 1$, the shadows from different inclusions overlap and the volume of the specimen in which the distortions occur no longer increases linearly with the field. Although at this point a departure from linearity might be expected, it was not observed by RGN, even at fields well beyond this limit.

We also remark that as f approaches the critical percolation fraction f_c the extra dissipation (at a fixed field) reaches a maximum and then decreases, reaching zero when $f=f_c$. This behavior is a simple volume effect; the reduction in the resistivity caused by the presence of superconducting material eventually exceeds the increase in resistivity induced by current distortions. The explicit dependence of ρ on f as $f\to f_c$ cannot be obtained easily from our model but has been calculated recently by Stroud.[10]

ACKNOWLEDGMENTS

It is a pleasure to thank Professor D. Stroud for helpful conversations and Mr. K. Loeffler for assistance with the computer programming. This work was supported in part by National Science Foundation Department of Materials Research Grants Nos. (DMR) 8106121 (J.C.G) and 8305473 (R.S.N). The Ohio State Unversity Materials Research Laboratory (Grant No. DMR 8119368) provided some of the computation facilities.

APPENDIX: SUMMARY OF SOLUTIONS FOR ELECTRIC CURRENT DENSITY

In the following expressions, Σ, A, B, S, T, and V are as defined below:

$$\Sigma=\sinh^2\eta\sin^2\theta+\cosh^2\eta\cos^2\theta \ ,$$

$$A=\cos\phi+\beta\sin\phi \ ,$$

$$B=\sin\phi-\beta\cos\phi \ ,$$

$$S=\sinh\eta_0/Q_1(i\sinh\eta_0) \ ,$$

$$T=\frac{\cosh\eta_0}{Q_1^1(i\sinh\eta_0)} \ ,$$

$$V=\frac{1}{\cosh\eta}[Q_1^1(i\sinh\eta)\Sigma-2\tanh\eta\sin^{-2}\theta] \ .$$

(a) Transverse current injection ($\vec{J}\perp\vec{H}$):

$$J_x=J_0\left[1-\gamma\frac{TA^2V}{\Sigma}-\gamma TB^2\frac{Q_1^1(i\sinh\eta)}{\cosh\eta}\right] \ ,$$

$$J_y=\alpha ABT\frac{Q_1^1(i\sinh\eta)}{\cosh\eta}-\frac{V}{\Sigma} \ ,$$

$$J_z=\alpha J_0\gamma\frac{AT}{\Sigma}\sin\theta\cos\theta\,\mathrm{sech}\eta \ .$$

(b) Longitudinal current injection ($\vec{J}\,||\,\vec{H}$):

$$J_x=J_0\gamma^{1/2}\frac{SA}{\Sigma}\frac{\sin\theta\cos\theta}{\cosh\eta} \ ,$$

$$J_y=J_0\gamma^{1/2}SB\frac{\sin\theta\cos\theta}{\cosh\eta} \ ,$$

$$J_z=J_0\left[1-\frac{S}{\sinh\eta}\left[Q_1(i\sinh\eta)+\frac{\cos^2\theta}{\Sigma}\right]\right] \ .$$

---

*Present address: AT&T Bell Laboratories, Murray Hill, NJ 07974.

[1]S. A. Wolf and D. U. Gubser, Phys. Rev. Lett. 42, 324 (1979); Solid State Commun. 32, 449 (1979); S. A. Wolf, D. U. Gubser, W. W. Fuller, J. C. Garland, and R. S. Newrock, Phys. Rev. Lett. 47, 1071 (1981), and references therein.

[2]K. Epstein, A. M. Goldman, and A. M. Kadin, Phys. Rev. Lett. 47, 534 (1981).

[3]R. M. Boysel, A. D. Caplin, M. N. B. Dalimin, and C. N. Guy, Phys. Rev. B 27, 554 (1983).

[4]D. J. Resnick, J. C. Garland, and R. S. Newrock, Phys. Rev. Lett. 43, 1192 (1979); J. C. Garland, D. J. Resnick, and R. S. Newrock, in *Inhomogeneous Superconductors—1979 (Berkeley Springs, WV)*, Proceedings of the Conference on Inhomo-

geneous Superconductors, edited by D. U. Gubser, T. L. Francavilla, S. A. Wolf, and J. R. Leibowitz (AIP, New York, 1979), p. 251.

[5]D. Stroud, Phys. Rev. Lett. 44, 1708 (1980).

[6]J. B. Sampsell and J. C. Garland, Phys. Rev. B 13, 583 (1976).

[7]F. P. Esposito, R. S. Newrock, and K. Loeffler, Phys. Rev. Lett. 41, 818 (1978); Phys. Rev. B 20, 2348 (1978).

[8]For S/N composites both boundary conditions are on the electric potential, whereas for composites containing voids one boundary condition is on the normal component of the current at the normal-metal—void interface.

[9]R. Landauer, in *Electrical Transport and Optical Properties of Inhomogeneous Media (Ohio State University, 1977),* Proceedings of the First Conference on the Electrical Transport and Optical Properties of Inhomogeneous Media, edited by J. C. Garland and D. B. Tanner (AIP, New York, 1978), p. 2.

[10]D. Stroud and F. P. Pan, Phys. Rev. B 13, 583 (1976).

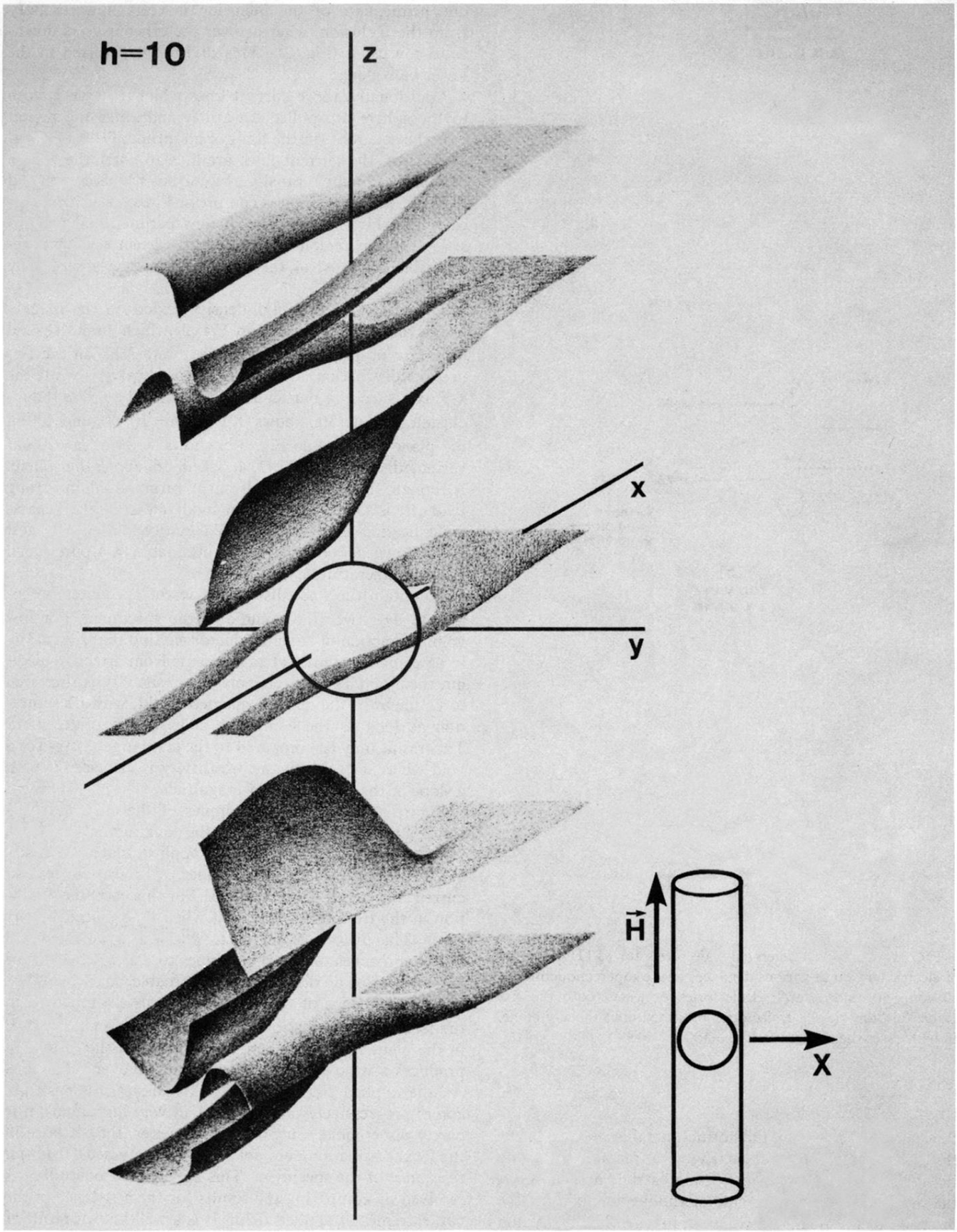

FIG. 2. Computer-generated isometric projection of several sheets of current for reduced field $h = 10$.

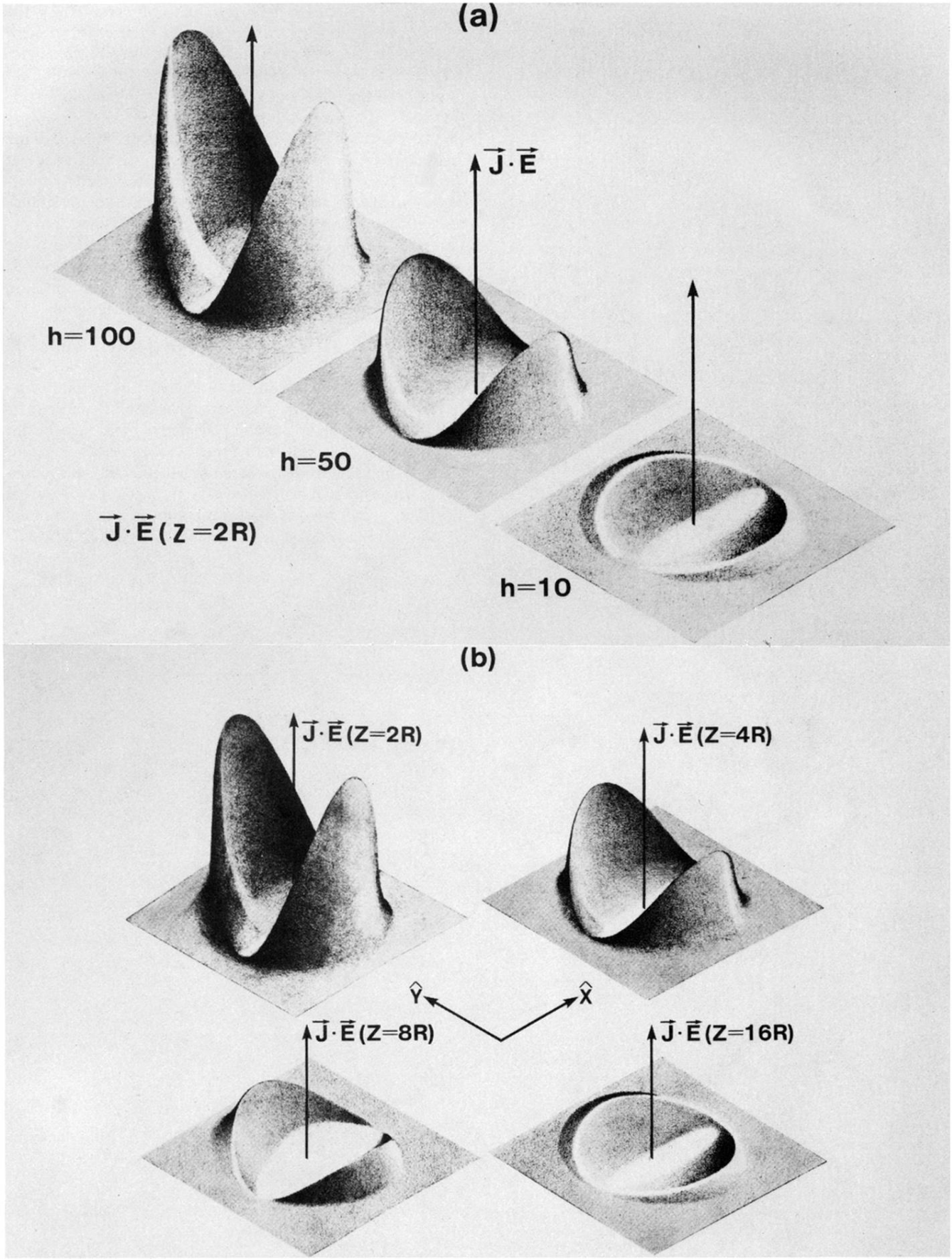

FIG. 3. Isometric projection of the power dissipated ($\vec{J}\cdot\vec{E}$) in the neighborhood of the inclusion for the transverse case. (a) $\vec{J}\cdot\vec{E}$ for various h in the plane $z=2$; (b) $\vec{J}\cdot\vec{E}$ for various z at $h=100$.

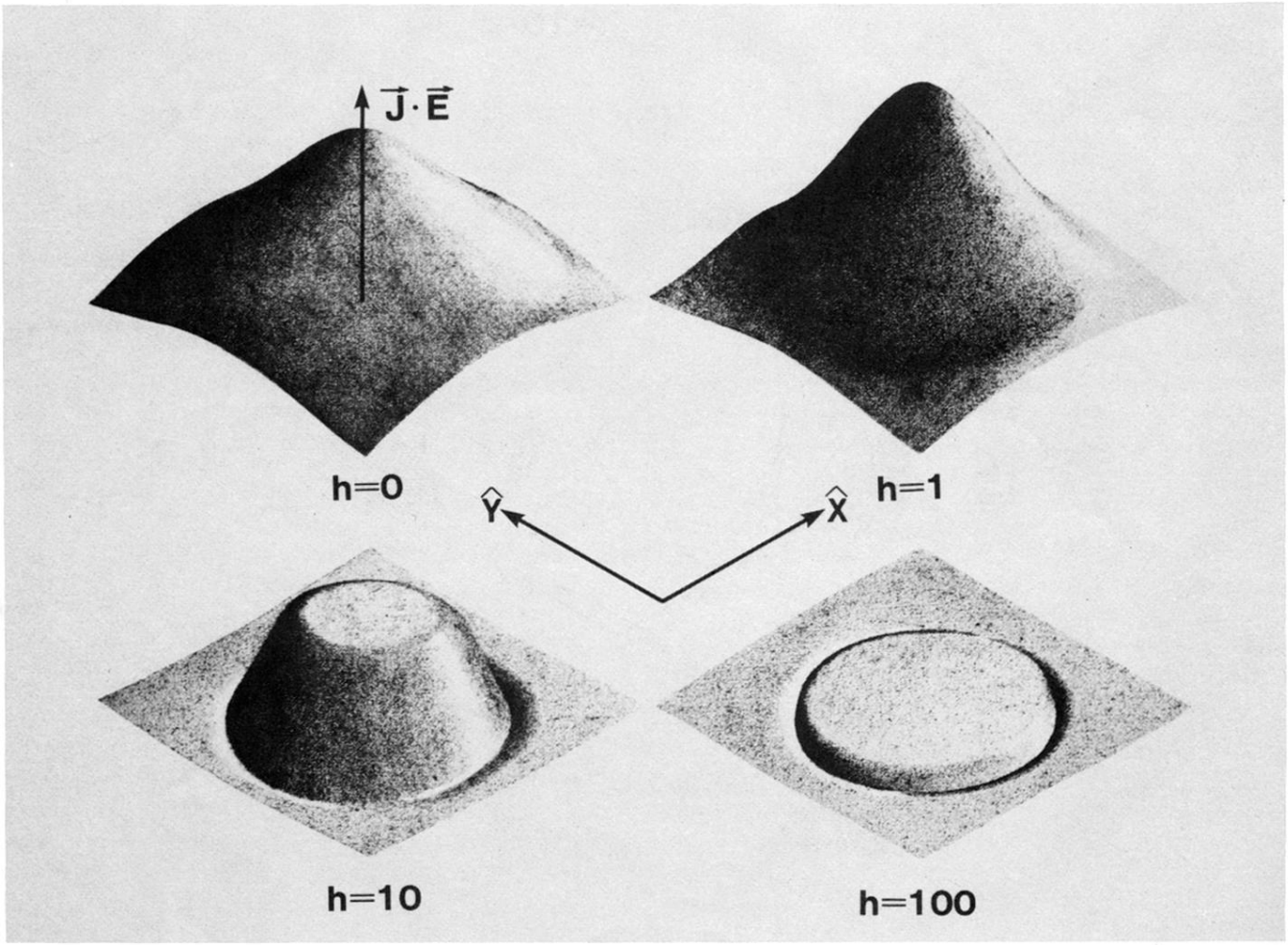

FIG. 5. Isometric projection of the dissipation $\vec{J}\cdot\vec{E}$ in the neighborhood of the inclusion for the longitudinal case.